

# Structural Basis of the Sensor-Synthase Interaction in Autoinduction of the Quorum Sensing Signal DSF Biosynthesis

Zhihong Cheng,<sup>1,5</sup> Ya-Wen He,<sup>1,5</sup> Siew Choo Lim,<sup>1,2,5</sup> Rohini Qamra,<sup>1,5</sup> Martin A. Walsh,<sup>3</sup> Lian-Hui Zhang,<sup>1,4,\*</sup> and Haiwei Song<sup>1,2,4,\*</sup>

<sup>1</sup>Institute of Molecular and Cell Biology, 61 Biopolis Drive, Proteos, Singapore 138673

<sup>2</sup>School of Biological Sciences, Nanyang Technological University, 60 Nanyang Drive, Singapore 637551

<sup>3</sup>MRC France, CRG BM14, ESRF, B.P.220, F-38043 Grenoble CEDEX, France

<sup>4</sup>Department of Biological Sciences, National University of Singapore, 14 Science Drive, Singapore 117543

<sup>5</sup>These authors contributed equally to the work

\*Correspondence: [lianhui@imcb.a-star.edu.sg](mailto:lianhui@imcb.a-star.edu.sg) (L.-H.Z.), [haiwei@imcb.a-star.edu.sg](mailto:haiwei@imcb.a-star.edu.sg) (H.S.)

DOI 10.1016/j.str.2010.06.011

## SUMMARY

The diffusible signal factor (DSF)-dependent quorum sensing (QS) system adopts a novel protein-protein interaction mechanism to autoregulate the production of signal DSF. Here, we present the crystal structures of DSF synthase RpfF and its complex with the REC domain of sensor protein RpfC. RpfF is structurally similar to the members of the crotonase superfamily and contains an N-terminal  $\alpha/\beta$  spiral core domain and a C-terminal  $\alpha$ -helical region. Further structural and mutational analysis identified two catalytic glutamate residues, which is the conserved feature of the enoyl-CoA hydratases/dehydratases. A putative substrate-binding pocket was unveiled and the key roles of the residues implicated in substrate binding were verified by mutational analysis. The binding of the REC domain may lock RpfF in an inactive conformation by blocking the entrance of substrate binding pocket, thereby negatively regulating DSF production. These findings provide a structural model for the RpfC-RpfF interaction-mediated QS autoinduction mechanism.

## INTRODUCTION

A quorum sensing mechanism allows bacteria to sense their population density and synchronize individual behavior into cooperative community behavior (Bassler and Losick, 2006; Von Bodman et al., 2003; Zhang and Dong, 2004) which provides bacterial pathogens an obvious competitive advantage over their hosts in pathogen-host interaction. The most critical feature of quorum sensing (QS) could be the molecular mechanism that enables bacterial cells to autoregulate the production of QS signals. In the QS system of *Vibrio fischeri*, which is considered as the paradigm of QS in Gram-negative bacteria (Milton, 2006; Whitehead et al., 2001), the QS signal AHL functions as a ligand to its cognate transcription factor LuxR. At low population density, each cell in the bacterial population produces a basal

level of AHL signals via the AHL-synthase LuxI. When a “quorum” population density is reached, the accumulated AHL signals interact with LuxR proteins; the resultant AHL-LuxR complex activates the transcriptional expression of the QS-dependent genes as well as the *luxI* gene, leading to the boosted production of AHL signals (Dong et al., 2007). This elegant signal autoinduction mechanism enables bacterial cells to sense their population density, to synchronize the expression of QS-regulon within the community in an effective way, and allows resetting of the QS circuit when a portion of bacterial cells are transferred to a new environment.

In addition to the well-characterized AHL-type QS system, a diffusible signal factor (DSF)-dependent QS system has recently been identified in a range of plant and human bacterial pathogens (Barber et al., 1997; Boon et al., 2008; Colnaghi Simionato et al., 2007; Fouhy et al., 2007; Huang and Wong, 2007; Wang et al., 2004). The DSF-type QS system, which plays a key role in regulation of bacterial virulence in various pathogens, was initially discovered from bacterial pathogen *Xanthomonas campestris* pv. *campestris* (*Xcc*) (Barber et al., 1997). Genetic and biochemical analyses show that the pathogen has evolved a novel form of autoregulation mechanism that allows DSF, which has been characterized as *cis*-11-methyl-2-dodecenoic acid, to autoregulate its biosynthesis (He et al., 2006a). This autoinduction mechanism involves two proteins, i.e., the DSF synthase RpfF and the membrane-associated DSF sensor RpfC. Mutation of *rpfF* abolishes DSF production and results in reduced virulence factor production (Barber et al., 1997; He et al., 2006b), whereas disruption of *rpfC* resulted in contrasting phenotypes. The *rpfC* mutant synthesizes about 16-fold higher DSF signal than the wild-type *Xcc* but produces significantly reduced virulence factors in a level similar to the *rpfF* mutant (Wang et al., 2004). Similar to the AHL-type QS signal production, the DSF level in *Xcc* increases proportionally following the increment of bacterial population density (Barber et al., 1997; Wang et al., 2004). However, the transcript level of *rpfF* remains more or less constant throughout growth and is not influenced by exogenous addition of DSF (Barber et al., 1997; He et al., 2006b), suggesting that autoregulation of DSF biosynthesis unlikely occurs at the transcriptional level.

RpfC is a hybrid sensor consisting of multidomains including a transmembrane domain, a histidine kinase (HK) domain,

a CheY-like receiver (REC) domain, and a histidine phosphotransferase (HPT) domain. Knocking out *rpfC* results in decreased virulence factor production but enhanced DSF biosynthesis (Slater et al., 2000; Wang et al., 2004). Our recent study has shown that mutation of the key residues implicated in phosphorelay in RpfC decreases virulence factor but has no effect on DSF production, whereas overexpression of its REC domain alone abolishes DSF biosynthesis (He et al., 2006a). In addition, coimmunoprecipitation and far western analysis showed that RpfF binds specifically to the REC domain of RpfC (He et al., 2006a). These findings suggest a model in which RpfC employs two different mechanisms to regulate virulence factor and DSF production simultaneously; i.e., the hybrid sensor relies on the conserved phosphorelay mechanism and its cognate response regulator RpfG to induce the expression of virulence genes, and suppresses DSF biosynthesis by its REC domain via a novel mechanism involving the RpfC/RpfF interaction.

In order to investigate the mechanism of how DSF autoinduction is mediated by the RpfF/RpfC interaction, we determined the crystal structures of full-length RpfF alone and in complex with the REC domain of RpfC. RpfF in complex with the REC domain adopts a crotonase-like fold, which consists of four C-terminal helices, that is essentially same as that observed in its apo form. The binding of the RpfC REC domain appears to block ligand entrance to the active site of RpfF, thereby negatively regulating DSF production. Structural comparison combined with mutagenesis sheds light on the mechanism that governs DSF autoinduction and further enriches our understanding on the diversity of bacterial QS systems.

## RESULTS

### Structure Determination

The crystal structure of full-length RpfF has been solved by the single-wavelength anomalous dispersion (SAD) method at a resolution of 1.8 Å. There are three polypeptide chains per asymmetric unit (AU) with a three fold noncrystallographic symmetry (NCS) axis. Residues of 1–13, 34–41, and 279–289 are disordered in all three chains of RpfF. The three subunits are virtually identical and can be superimposed upon one another with an average root mean square deviation (rmsd) less than 0.3 Å.

The crystal structure of full-length RpfF in complex with the REC domain of RpfC (designated as RpfF/REC) has been determined at a resolution of 2.5 Å by molecular replacement using the structure of RpfF as the search model. A representative portion of the initial electron density map in the region of the RpfC REC domain is shown in Figure S1 (available online). The final model of the RpfF/REC complex contains three complexes in the AU (RpfF: chains A, B, and C; REC: chains D, E, and F), which are related by a 3-fold NCS axis. Residues of 1–13, 34–41, and 279–289 in each subunit of the RpfF molecules are disordered. Residues of 449–461, 484–486, and 582–590 in chain D, residues of 449–461, 481–486, and 581–590 in chain E, and residues of 449–461, 482–486, and 582–590 in chain F are disordered. Since no substantial differences are observed between the three complexes in the AU (pairwise rmsd values of 0.42 and 0.44 Å for RpfF and REC, respectively, when all the equivalent C $\alpha$  atoms are superimposed), all the subsequent analysis uses the coordi-

**Table 1. Data Collection and Refinement Statistics**

	RpfF	RpfF/REC
Data Collection		
Derivative	SeMet	—
Wavelength (Å)	0.9795	0.9795
Resolution limit (Å)	1.8	2.5
Space group	P2 <sub>1</sub> 2 <sub>1</sub> 2 <sub>1</sub>	P6 <sub>5</sub>
Cell parameters		
a/b/c (Å)	96.8/112.3/119.6	130.9/130.9/156.5
$\alpha/\beta/\gamma$ (°)	90/90/90	90/90/120
Unique reflections (N)	117918	35459
I/ $\sigma$	11.3 (2.9)	11.5 (2.5)
Completeness (%)	97.5 (85.2)	99.4 (99.8)
R <sub>merge</sub> <sup>a</sup>	0.094 (0.314)	0.068 (0.418)
Number of Se sites	14	—
Anomalous phasing power	1.46	
Figure of merit	0.45/0.92	
Before/after density modification		
Refinement Statistics		
Data range (Å)	30.0–1.8	20.0–2.5
Used reflections (N)	111,882	56,289
Nonhydrogen atoms	6142	8680
R <sub>work</sub> <sup>b</sup> (%)	22.8	24.7
R <sub>free</sub> <sup>c</sup> (%)	24.7	27.8
Rmsd		
Bond length (Å)	0.002	0.004
Bond angles (°)	0.432	0.72
Ramachandran plot (% residues)		
Allowed	99.7	96.0
Generously allowed	0.3	3.7
Disallowed	0	0.3

Values in parentheses indicate the specific values in the highest resolution shell.

<sup>a</sup> R<sub>merge</sub> =  $\sum |I_i - \langle I \rangle| / \sum I_i$ , where  $I_i$  is the intensity of an individual reflection, and  $\langle I \rangle$  is the average intensity of that reflection.

<sup>b</sup> R<sub>work</sub> =  $\sum ||F_o| - |F_c|| / \sum |F_c|$ , where  $F_o$  denotes the observed structure factor amplitude, and  $F_c$  denotes the structure factor amplitude calculated from the model.

<sup>c</sup> R<sub>free</sub> is as for R<sub>work</sub> but calculated with 5.0% of randomly chosen reflections omitted.

nates of chain A of RpfF and chain D of the REC domain. Statistics of structure determination and refinement are summarized in Table 1 (see Experimental Procedures).

### Overall Architectures of RpfF and the REC Domain of RpfC

RpfF, in both free form and in complex with the REC domain of RpfC, adopts essentially the same fold with the rmsd of 0.42 Å when all the C $\alpha$  atoms from both forms are superimposed. As shown in Figures 1A and 1B, RpfF contains an N-terminal spiral core domain and a C-terminal  $\alpha$ -helical region. The spiral fold in RpfF contains four turns, each of which consists of three continuous secondary structure elements, namely, two  $\beta$  strands

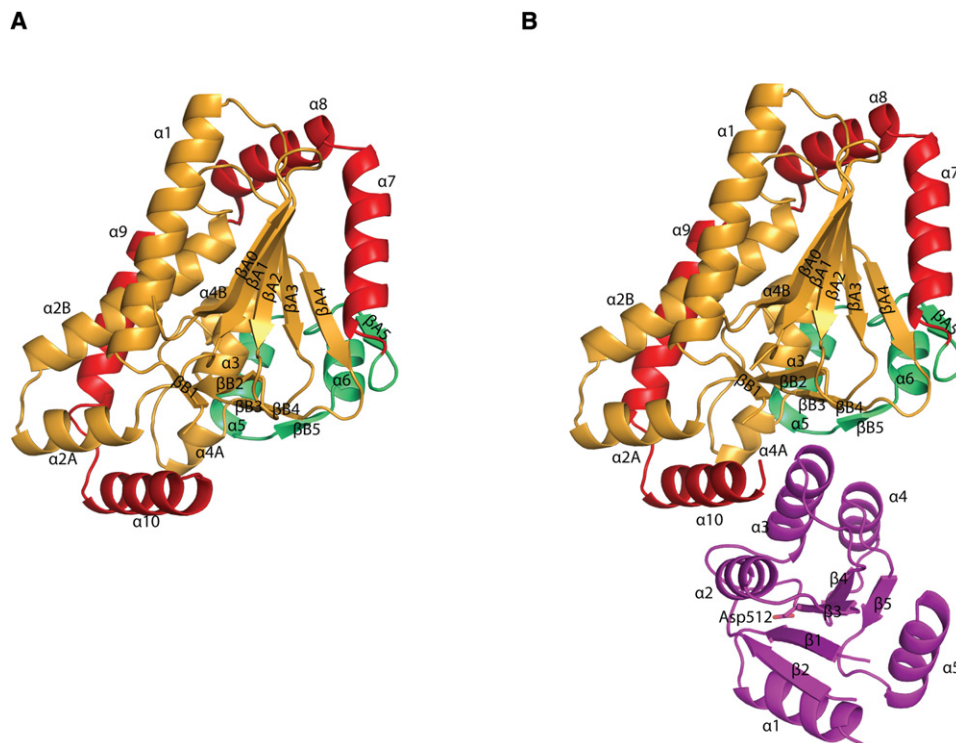


**Figure 1. Structure of RpfF Alone and in Complex with the REC Domain of RpfC**

Ribbon diagrams showing the self-association fold of RpfF (A) and the overall structure of the RpfF/REC complex (B). The N-terminal  $\alpha/\beta$  spiral domain is colored in orange, linker region in green, and the C-terminal  $\alpha$ -helical region in red. The REC domain of RpfC is shown in magenta with residue Asp512 in stick model. See Figure S1, which shows a representative portion of the Fo-Fc electron density map for the RpfC REC domain that is missing in the search model.

and one  $\alpha$  helix. Two  $\beta$  strands of each turn are categorized into two parallel  $\beta$  sheets separately, named  $\beta$  sheet A and B. Thus, after the very beginning  $\beta$ A0, which antiparallels with  $\beta$  sheet A, the following spiral core domain contains four turns:  $\beta$ A1/ $\beta$ B1/ $\alpha$ 1,  $\beta$ A2/ $\beta$ B2/ $\alpha$ 2B/ $\alpha$ 2A,  $\beta$ A3/ $\beta$ B3/ $\alpha$ 3, and  $\beta$ A4/ $\beta$ B4/ $\alpha$ 4B/ $\alpha$ 4A. The link region between N-terminal spiral fold and C-terminal  $\alpha$  helix consists of two  $\alpha$  helices ( $\alpha$ 5 and  $\alpha$ 6) interspersed with two  $\beta$  strands ( $\beta$ B5, antiparalleled with  $\beta$  sheet B, and  $\beta$ A5 lined up with  $\beta$  sheet A in parallel). The C-terminal  $\alpha$ -helical domain is composed of four  $\alpha$  helices wrapping around the spiral fold successively in such a way that  $\alpha$ 7 and  $\alpha$ 10 are facing the outer faces of  $\beta$  sheets A and B, respectively, with  $\alpha$ 8 and  $\alpha$ 9 in between.

The REC domains are the dominant molecular switches in bacterial two components signaling pathways. Several structures of nonphosphorylated REC domains (Baikalov et al., 1996; Djordjevic and Stock, 1998; Feher et al., 1997; Sola et al., 1999; Stock et al., 1989; Volkman et al., 1995), and two of phosphorylated REC domains have been determined (Casino et al., 2009; Kern et al., 1999). These structures indicated that the REC domains share a common fold and phosphorylation induced a large conformational change. As expected, the REC domain of RpfC in the RpfF-REC complex adopts a similar  $5\alpha/5\beta$  fold: parallel  $\beta$  sheet ( $\beta$ 2/ $\beta$ 1/ $\beta$ 3/ $\beta$ 4/ $\beta$ 5) surrounded by three helices ( $\alpha$ 2/ $\alpha$ 3/ $\alpha$ 4) on one side and two helices ( $\alpha$ 1/ $\alpha$ 5) on the other side (Figure 1B). The phosphoacceptor Asp512 of the REC domain is located on the loop  $\beta$ 3- $\alpha$ 3. Structural comparison

showed that a  $Mg^{2+}$  from the crystallization buffer occupies the position of the phospho-group and is coordinated with residues Asp468, Asp469, Lys566, and His514.

#### RpfF Belongs to the enoyl-CoA Hydratase/Isomerase Family

A search of Protein Data Bank using the Dali server revealed more than 50 structural homologs with high Z-score ( $>20$ ), all belonging to the crotonase superfamily. The homologs with solved crystal structures include rat mitochondrial enoyl-CoA hydratase (Engel et al., 1996, 1998) (PDB: 1DUB/2DUB, Z-score 21.2), 4-(N, N-dimethylamino) cinnanoyl-CoA hydratase (Bahson et al., 2002) (PDB: 1EY3, Z-score 21.5), hexanoyl-CoA hydratase (Bell et al., 2002) (PDB: 1MJ3, Z-score 21.2), human AU-rich RNA-binding protein/3-hydroxy-3-methylglutaconyl-CoA hydratase (Kurimoto et al., 2001) (PDB: 1HZD, Z-score 26.7), human mitochondrial  $\Delta$ 3- $\Delta$ 2-enoyl-CoA isomerase (Partanen et al., 2004) (PDB: 1SG4, Z-score 26.9), and *Saccharomyces cerevisiae*  $\Delta$ 3- $\Delta$ 2-enoyl-CoA isomerase (Mursula et al., 2001) (PDB: 1HNU, Z-score 22.9). Although RpfF shares relatively low sequence identity ( $<25\%$ ) with the members of enoyl-CoA hydratase/isomerase subfamily, superposition of the equivalent  $C\alpha$  atoms of RpfF with the members of the subfamily gives pairwise rmsd values of 1.5–1.8 Å, suggesting that RpfF belongs to the enoyl-CoA hydratase/isomerase family.

Interestingly, the last two helices ( $\alpha$ 9 and  $\alpha$ 10) of all available enoyl-CoA hydratase structures with bound ligands do not

wrap around the spiral core domain (Figure S2) but flip upward and attach to  $\alpha 8$  to form a T2 trimerization domain (Kurimoto et al., 2001). RpfF and enoyl-CoA hydratase have a common N-terminal core domain but differ in the C-terminal domain fold in that helices  $\alpha 9$  and  $\alpha 10$  of RpfF join  $\alpha 7$  and  $\alpha 8$  to wrap around the spiral core domain (Figure S2). RpfF is also similar to enoyl-CoA isomerases (PDB code: 1SG4) either in ligand bound form or in free form, in which the last four helices in the C-terminal region wrap around the spiral core domain, forming a so-called self-association fold (Figure S2) (Hubbard et al., 2005).

### RpfF Resembles an enoyl-CoA Hydratase Containing Two Conserved Catalytic Glutamate Residues

The exact role of RpfF in DSF biosynthesis remains unclear. Previous structural and functional studies have demonstrated that enoyl-CoA hydratases contain two catalytic glutamates while enoyl-CoA isomerase only contains one catalytic glutamate and the other glutamate is substituted by a Leu residue (Bahnon et al., 2002; Engel et al., 1996, 1998; Muller-Newen et al., 1995). Sequence alignment of RpfF with the enoyl-CoA hydratases and enoyl-CoA isomerase (Figure S3) indicated that, like enoyl-CoA hydratase, RpfF harbors two well-conserved glutamate residues Glu141 and Glu161, which correspond to the catalytic residues Glu144 and Glu164 in enoyl-CoA hydratase, respectively (PDB code: 2DUB) (Bahnon et al., 2002). In contrast, only Glu161 of RpfF aligns with Glu136 of enoyl-CoA isomerase, whereas Glu141 of RpfF corresponds to Leu114, which is not required for catalysis in enoyl-CoA isomerase (Partanen et al., 2004). This result suggests that RpfF is likely an enoyl-CoA hydratase rather than an enoyl-CoA isomerase. Further support to this notion comes from structural superposition of the putative active site of RpfF with those of enoyl-CoA hydratases/isomerase. As shown in Figure 2A, the active site of enoyl-CoA hydratases is composed of  $\alpha 3$ ,  $\beta B2-\alpha 2B$  loop,  $\beta B3-\alpha 3$  loop,  $\beta B4-\alpha 4B$  loop, and  $\alpha 9'$  and  $\alpha 10'$  from its neighboring molecule. Previous functional and structural studies showed that two highly conserved glutamate residues Glu144 from  $\alpha 3$  and Glu164 from the  $\beta B4-\alpha 4B$  loop are critical for their hydratase activity with Glu164 acting as a proton donor while Glu144 activating a water molecule to add the hydroxyl group to substrate (Bahnon et al., 2002; Engel et al., 1996, 1998; Muller-Newen et al., 1995). Close inspection of the catalytic site shows that residues Glu141 and Glu161 in RpfF spatially align well, respectively, with the catalytic residues Glu144 and Glu164 from the enoyl-CoA hydratases. Consistent with these findings, point mutation of Glu141 or Glu161 completely abolished DSF production, underscoring the critical roles of these two residues in DSF biosynthesis (Figure 2B). Taken together, these results suggest that RpfF likely belongs to the enoyl-CoA hydratase subfamily with two key glutamate residues in its catalytic site.

### RpfF Contains a Hydrophobic Pocket which Is Probably a DSF Precursor Docking Site

In addition to these two critical catalytic residues Glu141 and Glu161, other important residues in the catalytic site are also highly conserved between RpfF and enoyl-CoA hydratases (Figure 2A; Figure S3). For example, Leu136 from  $\beta B3$ , Gly137 and Gly138 from  $\beta B3-\alpha 3$  loop, Gly85 from  $\beta B2-\alpha 2B$  loop, and

Leu276 from  $\alpha 10$  may coordinate the substrate binding as well as catalytic activity. Residue Met170 from  $\beta B4-\alpha 4B$  loop and Trp258 from  $\alpha 9$  are hydrophobic and may contact the long fatty acyl group of the DSF precursor molecule. All of these residues are highly conserved across different homologs of RpfF (Figure S3) and form a hydrophobic pocket (Figures 2C). This pocket is similar to the substrate binding pockets in rat enoyl-CoA hydratase (Bahnon et al., 2002) and methylmalonyl decarboxylase (Benning et al., 2000) but too small to accommodate the 13 carbon fatty acyl chain of a DSF molecule since the dimethyl group of this molecule sterically clashes with  $\alpha 9$  of RpfF. Moreover, we observed that helix  $\alpha 10$  also clashes with the CoA moiety of the superimposed ligands (Figure 2C; see below). Altogether, these observations suggest that this cavity is probably a DSF precursor docking site and that RpfF may undergo a conformational change to relieve the steric hindrance for accommodating the incoming substrate.

To examine the role of the residues in the putative substrate binding pocket in RpfF, mutagenesis was performed on these residues and the resultant variant RpfF were expressed in the DSF-deficient strain  $\Delta rpfF\Delta rpfC$ . Consistent with the structural prediction, single point mutation in these residues resulted in either no DSF production or dramatically reduced DSF levels (Table S1), suggesting that these residues are important for DSF biosynthesis. Western blotting analysis confirmed that single point mutation did not affect RpfF protein expression level (data not shown).

### The RpfF/REC Interface

The interface between RpfF and REC domain involves the C-terminal helix  $\alpha 10$ ,  $\alpha 4A$ , the  $\beta$  sheet B of RpfF and helices  $\alpha 2$  and  $\alpha 3$  of the REC domain (Figure 1B). The interaction between these two proteins buries a pairwise accessible surface area of 1368 Å<sup>2</sup>. The interaction involves both hydrophilic and hydrophobic contacts. The C-terminal  $\alpha 10$  of RpfF contacts the surface groove of  $\alpha 2$  and  $\alpha 3$  of the REC domain to form a helix bundle mainly through hydrogen bond and polar interactions (Figure 3A). For example, Arg278 and Arg271 from  $\alpha 10$  of RpfF form hydrogen bonds with Asp499 and Glu495 of  $\alpha 2$  in the REC domain, respectively. Arg275 and Thr272 from  $\alpha 10$  of RpfF is hydrogen bonded to Gln526 in the  $\alpha 3$  of the REC domain, which in turn makes a polar contact with Asp522 in the same  $\alpha$  helix. The interface between  $\alpha 2$  and  $\alpha 3$  is composed of four hydrophobic residues Met518 and Leu498 from  $\alpha 2$ , and Met535 and Met530 from  $\alpha 3$ . On the other site, the  $\alpha 3$  of REC domain contacts the  $\beta$  sheet B mainly through hydrophobic interaction. As shown in Figure 3A, the side chain of Val529 and the methylene group of Arg528 contact the hydrophobic surface of RpfF composed of Leu136 from loop  $\beta B3-\alpha 3$ , Pro160 and Leu163 from  $\alpha 4A$ , and Leu194 from  $\beta B5$ . The residues involved in the interface are highly conserved across various bacterial species (Figures 3B and 3C), suggesting that the interaction of RpfF and the REC domain of RpfC is likely a conserved feature.

To verify the key structural features of RpfF that governs the RpfF-RpfC interaction, we first generated a truncated RpfF without C-terminal helix  $\alpha 10$ . The bacterial two-hybrid assay showed that the *Escherichia coli* strain coexpressing the truncated RpfF and REC domain could not grow in the selection

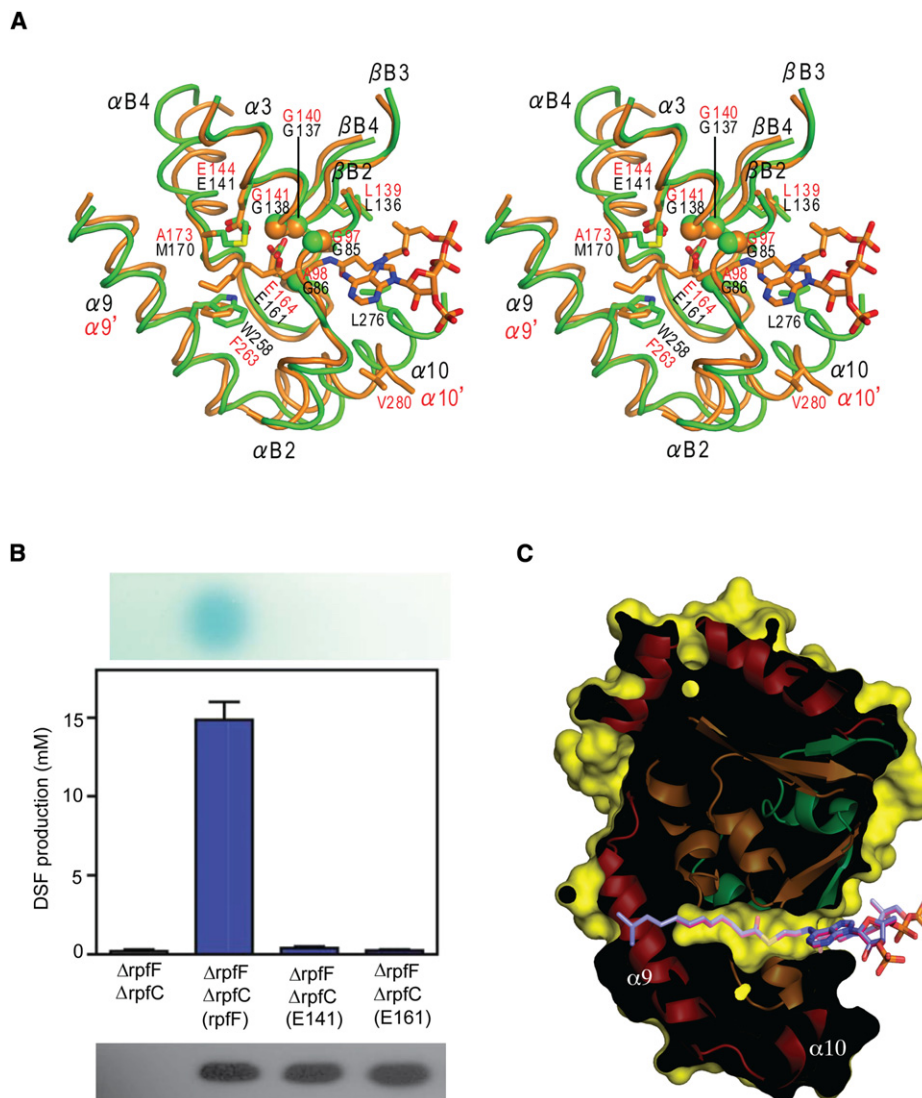


**Figure 2. Comparison of the Catalytic Site of RpfF and Octanoyl-CoA Hydratase**

(A) Stereo view of catalytic site of RpfF (green) superimposed with enoyl-CoA hydratase (PDB code: 2DUB, orange) in the presence of its ligand octanoyl-CoA shown in stick model. Glycine residues near active site are shown in spheres. Secondary structures and residues involved in catalytic site are labeled. See Figure S2 for structural comparison of RpfF with hydratase/isomerases, and Figure S3 for sequence alignment of RpfF and its homologs with enoyl-CoA hydratase (PDB: 2DUB) and isomerase (PDB: 1SG4).

(B) Mutagenesis reveals the critical residues involved in catalytic activity. Upper panel: TLC plate was used to quantify DSF activity as indicated by the presence of a blue zone. Middle panel: the amount of DSF production in WT and mutant RpfF. Lower panel: Western blot analysis to check expression of WT and mutant RpfF. The data are means of three repeats and error bars indicate SD.

See Table S1 for more information on mutational analysis of the residues associated with the putative substrate-binding pocket of RpfF.

(C) Cavity analysis of RpfF showed that the cavity in the putative catalytic site is too small to accommodate a substrate with the same carbon chain length as DSF (13 carbon atoms). The stick model in orange color is octanoyl-CoA from PDB code: 2DUB. The stick model in slate color is pre-DSF-CoA, which is modeled using the structure of octanoyl-CoA as a template, and is obviously larger than the cavity, suggesting that a conformation change will occur when RpfF binds to substrate.

screening medium (Figure 4A), suggesting that the C-terminal helix of RpfF plays a critical role in the interaction between RpfF and REC. In addition to the C-terminal helix  $\alpha$ -10, we have also tested the roles of residues Leu136, Pro160, Leu163, and Leu194 in the interaction. Our results showed that single point mutation in any of these residues had no effect on the interaction. However, double point mutations in Leu136 and Leu194

resulted in no binding of RpfF to REC domain (Figure 4A), which is consistent with our prediction that residues Leu136 and Leu194 are involved in the interface.

The involvement of the residues of the REC domain in binding to RpfF was also confirmed by using bacterial two hybrid assay. The *E. coli* strain coexpressing RpfF and the REC domain grow well on the selection medium; however, the *E. coli* strains

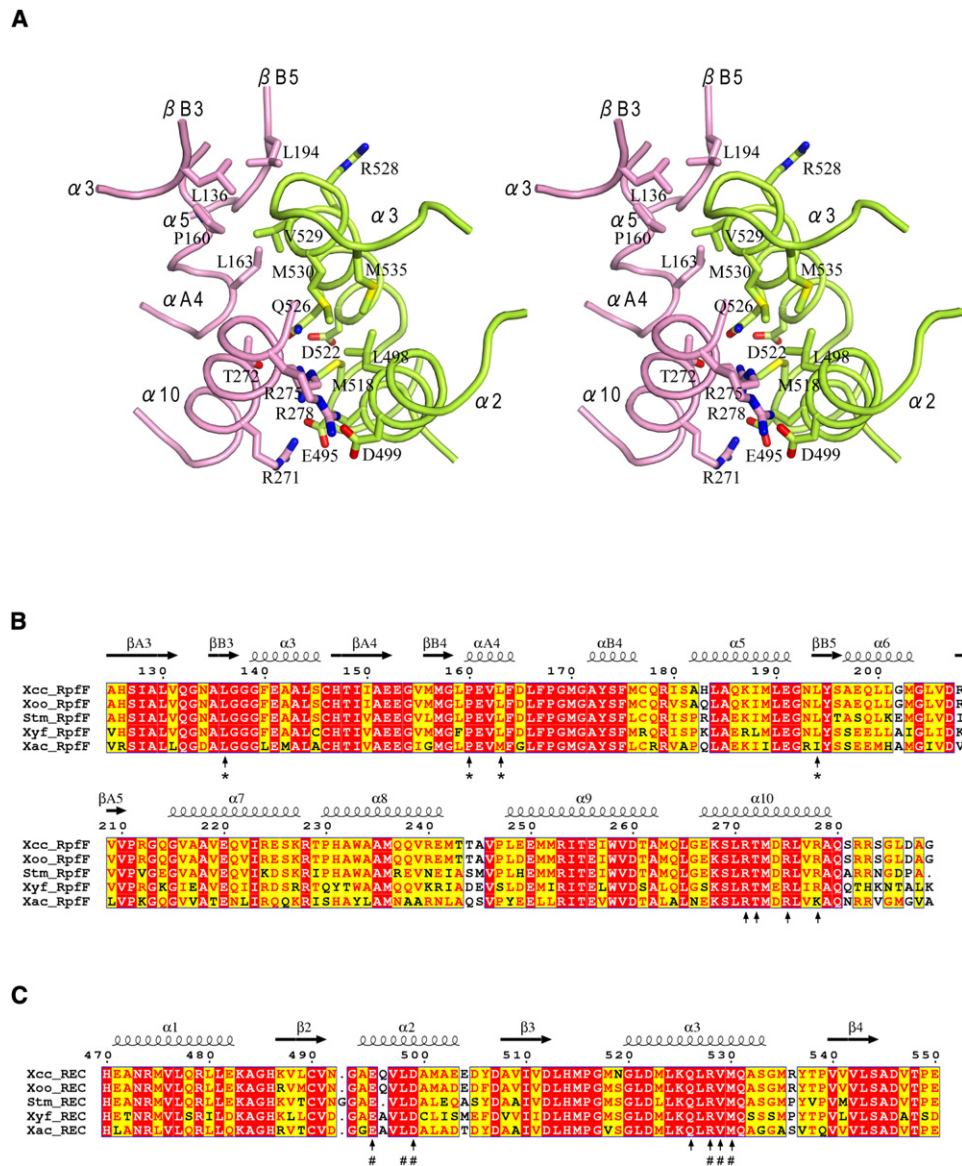


**Figure 3. Interaction between RpfF and the REC Domain of RpfC**

(A) Stereo view of the RpfF/REC interface. RpfF and the REC domain are shown in pink and lemon cartoon, respectively. Residues involved in the interactions are shown in stick models. Secondary elements and residues involved in the interface are labeled and indicated with “↑” in (B) and (C).

(B) Sequence alignment of RpfF and its homologs, *Xanthomonas oryzae* pv. *oryzae* (*Xoo*), *Stenotrophomonas maltophilia* (*Stm*), *Xylella fastidiosa* (*Xyf*), and *Xanthomonas axonopodis* pv. *citri* (*Xac*). Secondary structural elements are indicated. Mutated residues are marked with “\*.”

(C) Sequence alignment of the REC domain of RpfC from different bacterial species. Secondary structural elements are indicated. Mutated residues are marked with “#.”

coexpressing RpfF and the REC domain with triple mutations in Glu495, Leu498, and Asp499 or in Arg528, Val529, and Met530 failed to grow on the same selection screen medium (Figure 4A). The results of western blotting analysis precluded the possibility that the differences in growth were due to variation in protein expression level (Figure 4B).

To examine the functional role of the key residues of the REC domain in the interaction with RpfF, we created single or multiple point mutants in the REC domain and evaluated the mutational effects on DSF production. As shown in Figure 4C, deletion of

*rpfC* in *Xcc* resulted in overproduction of DSF and overexpression of REC domain in the mutant  $\Delta$ rpfC decreased the DSF biosynthesis by more than 97%. This is consistent with the notion that the binding between REC and RpfF blocks DSF biosynthesis. While a single point mutation in Leu498, Asp499, Arg528, or Met530 of REC did not affect DSF biosynthesis, substitution of Glu495 and Val529 with alanine substantially attenuated the inhibitory activity of REC on DSF production (Figure 4C). Moreover, double point mutations in Glu495 and Leu498, and triple point mutations in Glu495, Leu498, and

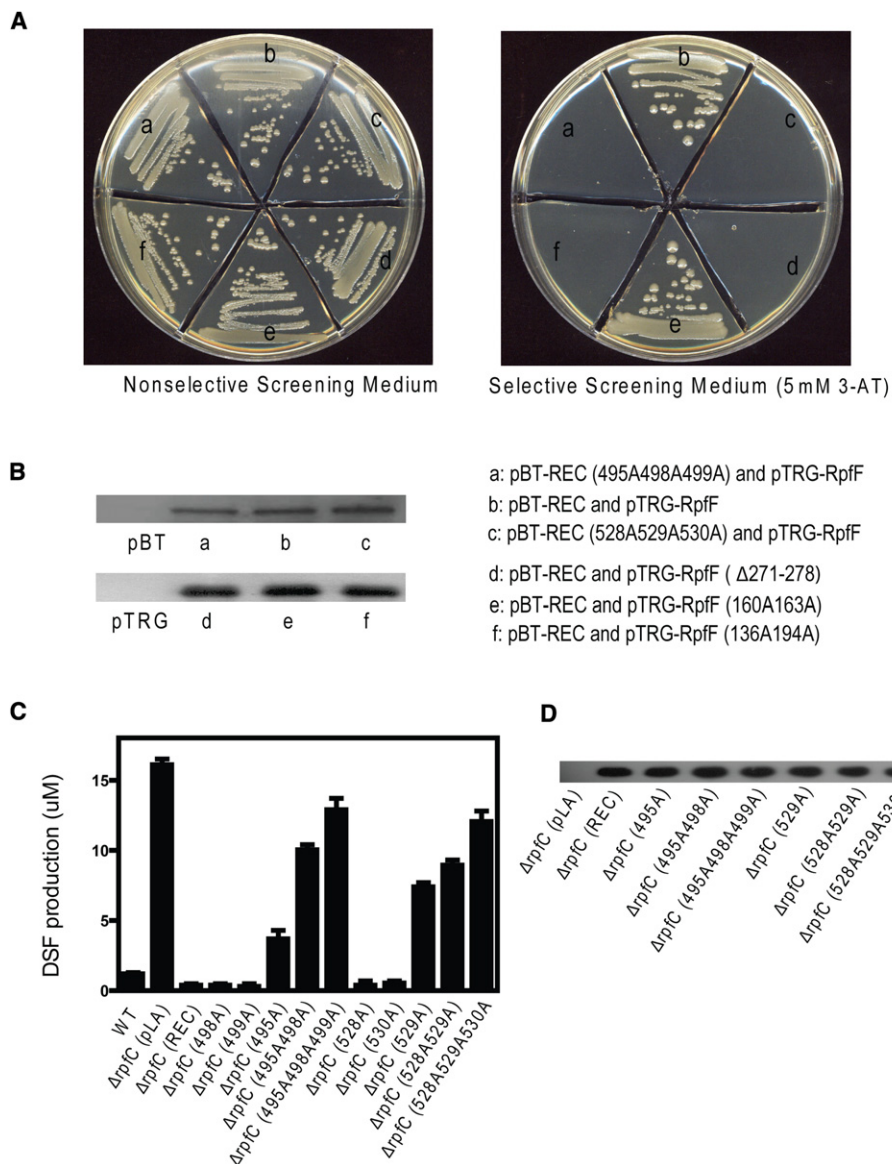


**Figure 4. Mutational Analysis of the Interface between RpfF and the REC Domain**

(A) Bacterial two-hybrid assay to confirm the roles of the predicted residues in the binding.

(B) Western blotting analysis to show the expression of variant REC or RpfF.

(C) DSF biosynthesis assay to verify the roles of the residues of REC domain in interaction with RpfF. The data are means of three repeats and error bars indicate SD.

(D) Western blotting to show that point mutation did not affect the expression of the REC domain.

Asp499 further compromised the REC inhibitory activity by up to 62% and 80%, respectively (Figure 4C). Similarly, the REC domain with double point mutations in Arg528 and Val529, triple point mutations in Arg528, Val529, and Met530 also resulted in loss of its DSF biosynthesis inhibitory activity by about 56% and 75%, respectively (Figure 4C). Western blotting analysis showed that the point mutations within REC did not affect the expression level of this domain (Figure 4D). Taken together, these data indicate that these residues are involved in the interface and work in a concerted way to mediate the interaction between RpfF and the REC domain.

### The REC Domain Appears to Lock RpfF in an Inactive State and Physically Blocks the Putative Substrate Binding Pocket

Based on the structure of RpfF apo form or in complex with RpfC REC domain, cavity analysis reveals that there is a closed cavity located in the catalytic site, which is too small to accommodate a CoA substrate with the length of DSF carbon chain (13 carbon atoms; Figure 2C) compared with the ligand octanoyl-CoA (PDB: 2DUB), suggesting that a conformation change may occur when the substrate binds to RpfF. Superimposition of RpfF in REC-bound form with those of hydratases and isomerases with bound

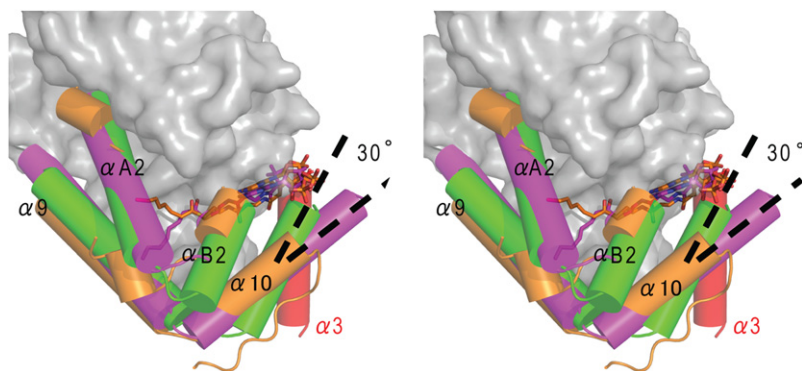


**Figure 5. Possible Conformational Changes of RpfF and the Inhibitory Effect of the REC Domain on Substrate Binding**

The stereo figure depicts the conformational change of helices of RpfF that are involved in catalytic site. Cylindrical cartoons of helix  $\alpha$ B2,  $\alpha$ A2,  $\alpha$ 9, and  $\alpha$ 10 of RpfF and other hydratases/isomerase (PDB code: 2DUB and 1SG4) are shown in green, magenta and orange, respectively. Ligands are shown in stick model with colors corresponding to their respective protein colors. The rest of RpfF is shown in gray solid surface while helix  $\alpha$ 3 of the REC domain is shown in red.

ligands reveals that conformational change occurs mainly in four helices:  $\alpha$ 9,  $\alpha$ 10,  $\alpha$ 2B, and  $\alpha$ 2A, which were highlighted in cylindrical cartoon in Figure 5. Helices  $\alpha$ 9 and  $\alpha$ 2A coordinate with the carbon chain of substrates, and different length of carbon chain may induce diversified conformational changes in these two helices. Thus, the binding of ligands with longer carbon chain would result in wide split between helices  $\alpha$ 2A and  $\alpha$ 9. Furthermore,  $\alpha$ 10 of RpfF in both apo- and REC-bound forms would clash with the CoA moiety if RpfF binds to a substrate. Such a steric hindrance would force  $\alpha$ 10 to rotate about  $30^\circ$  in the presence of a CoA-conjugated ligand (Figure 5). Besides  $\alpha$ 10 of RpfF, helix  $\alpha$ 3 of the REC domain also clashes with the CoA moiety of a substrate, suggesting that the REC domain itself would directly interfere the substrate binding to RpfF. Since the binding of RpfF to the REC domain is partially mediated by the interaction between  $\alpha$ 10 of RpfF and  $\alpha$ 3 of the REC domain, and  $\alpha$ 10 adopts an essentially same conformation in both apo- and REC-bound forms of RpfF, the binding of the REC domain may lock the position of  $\alpha$ 10 and force RpfF to stay an inactive form, thereby blocking substrate binding to the catalytic site.

## DISCUSSION

Evidence is accumulating that the DSF-dependent QS system of *Xcc* represents another family of widely conserved bacterial QS systems implicated in regulation of multiple biological functions. This system differs from other known QS systems in various aspects, in particular, the autoregulation mechanism that controls signal production (He and Zhang, 2008). Characterization of the protein structure of DSF synthase holds the key to understand how its catalytic activity can be modulated by its ligand protein RpfC. In this study, the crystal structure of the full-length RpfF, which is a key DSF synthase (Barber et al., 1997; Wang et al., 2004), was determined at a resolution of 1.8 Å. Structural comparison showed that RpfF has similar fold to the members of the enoyl-CoA hydratase/isomerase superfamily.

The common reaction mechanism of enoyl-CoA hydratases involves two catalytic glutamate residues (Hamed et al., 2008). We compared RpfF with the enoyl-CoA hydratase (PDB code: 2DUB), which is a well-characterized enzyme (Agnihotri and Liu, 2003; Bahnson et al., 2002). RpfF and 2DUB share two conserved catalytic glutamate residues (Glu141 and Glu161 in

RpfF), whose catalytic role in synthesis of DSF were verified by mutagenesis analysis. The C-terminal helices  $\alpha$ 9 and  $\alpha$ 10 of 2DUB do not form the self-association fold but interact with neighboring molecule and form an intratrimer association fold (Hubbard et al., 2005). In contrast, superposition of RpfF with the ligand-bound structures of 1EY3 reveals that the helices  $\alpha$ 9 and  $\alpha$ 10 of RpfF might act as an “arm” that can be flipped upward or away to allow ligand binding, or flipped downward to inhibit ligand binding. Presumably, RpfF may share a similar interfacial activation mechanism as the lipolytic enzymes, whose activation needs substrate aggregation or micelles to displace the helical “lid” that covers the catalytic site (Mingarro et al., 1995). These findings present useful clues for further characterization of the RpfF catalytic mechanisms and the precursor for DSF biosynthesis.

The most critical feature of a QS system is the mechanism that enables bacterial cells to autoregulate the production of QS signals. Our previous data show that *Xcc* has evolved a novel autoregulation mechanism involving the protein-protein interaction between RpfF and RpfC (He et al., 2006a). However, the mechanism by which RpfC modulates the RpfF enzyme activity and hence controls DSF production remains elusive. Structural comparison of the RpfF apo form and the RpfF-REC complex showed that RpfF appears to adopt the same “inactive” form in the absence or in the presence of the REC domain. In this inactive state, the C-terminal helix  $\alpha$ 10 of RpfF is orientated downward that blocks the entrance of the substrate-binding pocket as discussed above, and the helices  $\alpha$ 2 and  $\alpha$ 3 from the REC domain form a helix bundle with the  $\alpha$ -10 of RpfF to lock it in such a position that prevents interfacial activation. These structural findings not only provide plausible mechanistic explanation for how DSF autoinduction is mediated by the RpfF/RpfC interaction but also present further refinement for our previous proposed model of DSF autoinduction (He et al., 2006a) (Figure 6). At low cell density, RpfF is associated with the REC domain of RpfC, which might keep the DSF synthase in the inactive state and maintains the DSF production at a basal level (Figure 6A). When cell density reaches a threshold level, the diffusible DSF signals accumulate in extracellular environment and may interact with RpfC. The event presumably leads to phosphorylation of the REC domain and consequent release of RpfF, which catalyzes substantial DSF biosynthesis upon interfacial induction (Figure 6B).

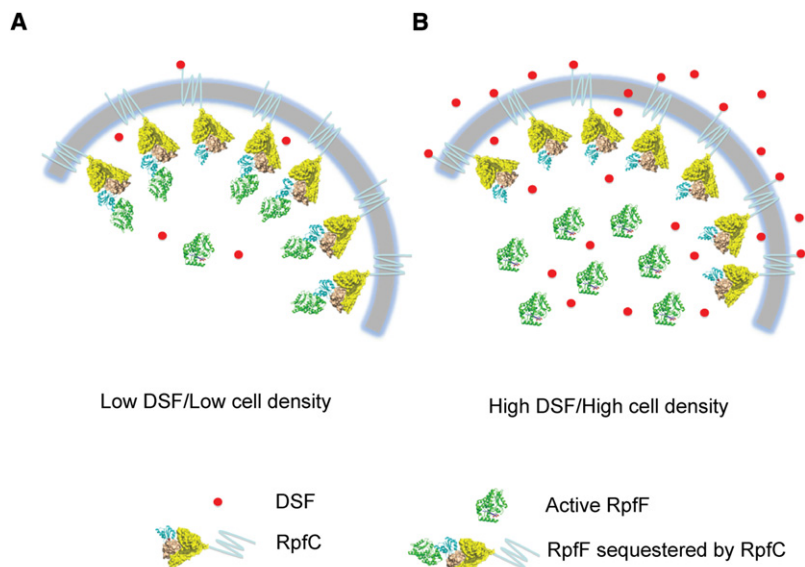


**Figure 6. Mechanism of DSF Autoinduction**

(A) In the case of low cell density, concentration of DSF is also very low, most of RpfF are sequestered by the RpfC REC domain and adopt an inactive form. A small group of RpfF is free from RpfC and is capable of DSF biosynthesis. (B) When cell grows and DSF accumulates to a certain threshold, DSF diffuses out of cell and binds to extracellular domain of RpfC, which triggers phosphorylation relay. Once the REC domain is phosphorylated, the interaction between RpfF and RpfC REC domain will be disrupted transiently. Thus, RpfF is released and able to bind to substrate and synthesize DSF. As the binding of substrate and the REC domain to RpfF seem to be mutually exclusive, RpfC can no longer sequester RpfF, which results in more DSF biosynthesis and downstream virulence regulation.

## EXPERIMENTAL PROCEDURES

### Bacterial Strains and Growth Conditions

Xcc strain XC1, and its derivatives FE 58 and  $\Delta$ rpfC, has been described previously (He et al., 2006a, 2006b; Wang et al., 2004). The double deletion mutant  $\Delta$ rpfF $\Delta$ rpfC was generated using  $\Delta$ rpfC as the parental strain following the method described previously (He et al., 2006a). Xcc strains were grown at 30°C in LB medium unless otherwise stated. *Escherichia coli* strains were maintained at 37°C in LB medium. Antibiotics were added at the following concentrations when required: kanamycin, 100  $\mu$ g/ml; ampicillin, 200  $\mu$ g/ml; rifampicin, 50  $\mu$ g/ml; tetracycline, 10  $\mu$ g/ml; chloramphenicol, 10  $\mu$ g/ml. X-gluc (5-bromo-4-chloro-3-indolyl  $\beta$ -D-glucopyranoside) was included in NYG medium at a final concentration of 30  $\mu$ g/ml for detection of GUS ( $\beta$ -glucuronidase) activity.

### Protein Expression and Purification

Full-length *rpfF* from Xcc was cloned into the vector pETDuet-1 with a N-terminal 6xHis tag. RpfF was expressed in *E. coli* strain BL21 (DE3) grown at 37°C in LB medium containing ampicillin. At  $OD_{600} = 0.6$ , cells were induced with 0.4 mM isopropylthio- $\beta$ -galactoside (IPTG) and grown at 18°C for an additional 16 hr prior to harvest. Cells were lysed in 25 mM Tris buffer (pH 8.0) with 500 mM NaCl and lysozyme. Cell debris was removed by centrifugation at 18,000 rpm at 4°C. The supernatant containing His-tagged RpfF was incubated with TALON resin (BD Biosciences) pre-equilibrated with the lysis buffer (25 mM Tris buffer [pH 8.0] and 500 mM NaCl). The column was washed with 15 mM imidazole, and protein was eluted with 100 mM imidazole. The protein was further purified by Superdex-200 gel filtration column (Amersham Biosciences). SeMet-substituted RpfF was expressed in a minimal medium containing 20 mg/l seleno-L-methionine (SeMet) and purified in the same way as the native protein.

To get the RpfF/REC complex, full-length RpfF and the REC domain (residues 449–590) of RpfC were cloned into the vector pETDuet-1 of multiple cloning sites-1 and -2, respectively, with a N-terminal 6xHis-Tag fused to RpfF. The complex was purified using TALON resin and Superdex 200 gel filtration columns. The eluted protein complexes were concentrated to ~15 mg/ml in a buffer containing 50 mM Tris-HCl (pH 8.0) and 100 mM NaCl for crystallization.

### Crystallization and Data Collection

For crystallization, RpfF was concentrated to 8 mg/ml in 25 mM Tris (pH 8.0), 500 mM NaCl, and 10 mM DTT. Crystallization screening was performed using the sitting-drop vapor-diffusion method at 15°C by mixing 200 nl protein solution with 200 nl reagent solution in 96-well plates using Phoenix liquid handling

robot. Rod-shaped crystals appear in 1 day from a reservoir solution of 0.2 M potassium thiocyanate and 20% (w/v) PEG 3350. This initial condition was then optimized to 0.2 M potassium thiocyanate and 9% (w/v) PEG 3350. Crystals suitable for data collection were grown in 48 hr by mixing 2  $\mu$ l protein solution with 2  $\mu$ l crystallization buffer, via the hanging-drop vapor-diffusion method. Crystals of SeMet-substituted RpfF were cryoprotected by 25% PEG 400 before flash-frozen in liquid nitrogen.

Crystals belong to P2<sub>1</sub>2<sub>1</sub>2<sub>1</sub> with cell parameters  $a = 96.8$  Å,  $b = 112.3$  Å,  $c = 119.6$  Å,  $\alpha = \beta = \gamma = 90^\circ$  and contains three molecules per asymmetric unit. SAD data sets were collected at 100 K from a single SeMet-labeled crystal using synchrotron radiation at beamline ID23-1 at the European Synchrotron Facility (ESRF), Grenoble, France.

Crystals of the RpfF/REC complex were grown at 15°C by hanging drop vapor diffusion. Equal volume of protein sample was mixed with the crystallization solution (100 mM MES-Na [pH 6.5], 20%–22% PEG4000, 200 mM MgCl<sub>2</sub>). Single crystals were transferred to the crystallization buffer with 20% ethylene glycol. Before being fast frozen in liquid nitrogen, crystals were quick soaked for less than 10 s in the cryo-buffer with 300 mM KI. Crystals belong to the space group P6<sub>5</sub> with cell parameters  $a = b = 130.9$  Å,  $c = 156.5$  Å,  $\alpha = \beta = 90^\circ$ , and  $\gamma = 120^\circ$  and contain three complexes per asymmetric unit. X-ray data were collected at ESRF, ID29 and processed with MOSFLM (Leslie, 1992).

### Structural Determination

The structure of RpfF was determined by the SAD method. The peak data were integrated using MOSFLM (Leslie, 1992) and processed with the CCP4i package (Potterton et al., 2003). Heavy atom search was carried out by SHELXC/D/E (Sheldrick, 2008). Model was built automatically by ARP/wARP (Morris et al., 2002). Crystallographic refinement was performed with the programs REFMAC5 (Murshudov et al., 1997) to a final  $R_{free}$  of 24.7%. The final refinement statistics for RpfF are summarized in Table 1.

The structure of RpfF/REC was determined by the molecular replacement method using program PHASER (McCoy et al., 2007) with the structure of RpfF as a search model. Three copies of RpfF in the AU were found sequentially with Z-scores 24.2, 46.4, and 58.5, respectively. Further molecular replacement trials searching for the REC domains of RpfC failed, but it was clearly shown in the difference Fourier maps. The partial mode of the REC domain was manually built using COOT (Emsley and Cowtan, 2004). Crystallographic refinement was carried out with REFMAC5 (Murshudov et al., 1997) with TLS and NCS restraints. The final refinement statistics for the complex are summarized in Table 1.

### Site-Directed Mutagenesis to Identify Key Residues Associated with DSF Biosynthesis and RpfF-RpfC Interaction

The coding sequences of *rpfF* and the REC domain of RpfC were amplified by PCR and cloned into the vector pGEM-T-easy (Promega), respectively. Point mutations were conducted using the QuickChange site-directed mutagenesis

kit following the manufacturer's instructions (Stratagene). The mutations were verified by DNA sequencing, and the primers used in PCR and mutagenesis are listed in Table S2. For identification of key residues associated with DSF biosynthesis, *rpfF* and its variants were cloned in the expression vector pLAFR3 and mobilized into double deletion mutant  $\Delta$ rpfF $\Delta$ rpfC for DSF production analysis using the method described below. Similarly, the coding sequence of REC domain and its variants were cloned in the same vector and introduced into the *rpfC* deletion mutant  $\Delta$ rpfC to verify the putative residues implicated in binding of RpfF. To identify the key residues of RpfF involved in binding to the REC domain, the construct pLAFR3 containing the coding region of REC domain and the construct pDSK519 containing RpfF or its variants were mobilized into the double deletion strain  $\Delta$ rpfF $\Delta$ rpfC for analysis of DSF production as described below.

### Quantification of DSF Production

Strain XC1 and its derivatives were grown in liquid LB medium until OD<sub>600</sub> reaching about 2.1. For each strain, the supernatants from 50 ml of cell cultures were collected by centrifugation at 10,000 rpm for 30 min. The supernatants were extracted twice by using equal volume of ethyl acetate. The organic phase was evaporated and the residues containing DSF were dissolved in 50  $\mu$ l of methanol. For DSF analysis, 5  $\mu$ l of crude extracts was spotted on TLC silica gel plate 60F<sub>254</sub> (Merck), which was separated in a tank containing ethyl acetate and Hexane (2:8, v:v) as eluting solvents. The TLC plate was air-dried and overlaid with 50 ml of NYG liquid medium supplemented with 0.8% agrose, 30  $\mu$ g/ml of X-gluc, and 1.5 ml of fresh DSF reporter strain FE58 (Wang et al., 2004). The TLC plate was incubated at 28°C in darkness overnight. DSF activity was indicated by the presence of a blue zone. For quantitative comparison, DSF concentration was calculated using the formula: DSF ( $\mu$ M) =  $0.0099e^{2.2527w}$ , based on the width (w) of blue zone in centimeter. The formula was derived from a dose-response plot of the biosensor using various dilutions of synthetic DSF signal, with a correlation coefficient ( $R^2$ ) of 0.9657.

### BacterioMatch II Two-Hybrid System to Evaluate RpfF and REC Binding

The RpfF and REC interaction was also detected using BacterioMatch II Two-hybrid system kit (Stratagene) following the manufacturer's instruction. In brief, *rpfF* and its variants were amplified using the primers listed in Table S2 and were fused separately with the gene  $\lambda$ cl encoding the full-length bacteriophage  $\lambda$  repressor protein (237 amino acids), containing the N-terminal DNA-binding domain and the C-terminal dimerization domain in the vector pBT. The coding sequences of REC domain and its derivatives were fused separately to the N-terminal domain of the  $\alpha$  subunit of RNA polymerase (248 amino acids) in the vector pTRG (Stratagene). The resultant constructs were cotransformed into the XL1-Blue RF' Kan strain. At the same time, the pTRG-Gal11P and the pBT-LGF2 positive control plasmids included in the kit were also cotransformed. The Nonselective Screening Medium (without 3-AT) was used for screening the *E. coli* colonies containing the cotransformed constructs. The growth of the selected strains was further verified on the Selection Screening Medium (5 mM 3-AT) by stripping. Normal growth on the Selection Screening Medium indicates a strong binding between two proteins. Western blotting analysis was used to confirm the expression of RpfF or REC.

### ACCESSION NUMBERS

The coordinates and structure-factor amplitudes of RpfF and the RpfF/REC complex have been deposited in the Protein Data Bank with accession codes 3M6N and 3M6M, respectively.

### SUPPLEMENTAL INFORMATION

Supplemental Information includes three figures and two tables and can be found with this article online at doi:10.1016/j.str.2010.06.011.

### ACKNOWLEDGMENTS

We thank the beamline scientists at ID-29 and ID23-1 (ESRF, France) for assistance and access to synchrotron radiation facilities. This work is financially

supported by the Biomedical Research Council of A\*STAR (Agency for Science, Technology and Research, Singapore) (H.S. and L.H.-Z.).

Received: April 13, 2010

Revised: June 17, 2010

Accepted: June 20, 2010

Published: September 7, 2010

### REFERENCES

- Agnihotri, G., and Liu, H.W. (2003). Enoyl-CoA hydratase: reaction, mechanism, and inhibition. *Bioorg. Med. Chem.* 11, 9–20.
- Bahnson, B.J., Anderson, V.E., and Petsko, G.A. (2002). Structural mechanism of enoyl-CoA hydratase: three atoms from a single water are added in either an E1cb stepwise or concerted fashion. *Biochemistry* 41, 2621–2629.
- Baikalov, I., Schroder, I., Kaczor-Grzeskowiak, M., Grzeskowiak, K., Gunsalus, R.P., and Dickerson, R.E. (1996). Structure of the Escherichia coli response regulator NarL. *Biochemistry* 35, 11053–11061.
- Barber, C.E., Tang, J.L., Feng, J.X., Pan, M.Q., Wilson, T.J., Slater, H., Dow, J.M., Williams, P., and Daniels, M.J. (1997). A novel regulatory system required for pathogenicity of Xanthomonas campestris is mediated by a small diffusible signal molecule. *Mol. Microbiol.* 24, 555–566.
- Bassler, B.L., and Losick, R. (2006). Bacterially speaking. *Cell* 125, 237–246.
- Bell, A.F., Feng, Y., Hofstein, H.A., Parikh, S., Wu, J., Rudolph, M.J., Kisker, C., Whitty, A., and Tonge, P.J. (2002). Stereoselectivity of enoyl-CoA hydratase results from preferential activation of one of two bound substrate conformers. *Chem. Biol.* 9, 1247–1255.
- Benning, M.M., Haller, T., Gerit, J.A., and Holden, H.M. (2000). New reactions in the crotonase superfamily: structure of methylmalonyl CoA decarboxylase from Escherichia coli. *Biochemistry* 39, 4630–4639.
- Boon, C., Deng, Y., Wang, L.H., He, Y., Xu, J.L., Fan, Y., Pan, S.Q., and Zhang, L.H. (2008). A novel DSF-like signal from Burkholderia cenocepacia interferes with Candida albicans morphological transition. *ISME J.* 2, 27–36.
- Casino, P., Rubio, V., and Marina, A. (2009). Structural insight into partner specificity and phosphoryl transfer in two-component signal transduction. *Cell* 139, 325–336.
- Colnaghi Simionato, A.V., da Silva, D.S., Lambais, M.R., and Carrilho, E. (2007). Characterization of a putative Xylella fastidiosa diffusible signal factor by HRGC-El-MS. *J. Mass Spectrom.* 42, 490–496.
- Djordjevic, S., and Stock, A.M. (1998). Structural analysis of bacterial chemotaxis proteins: components of a dynamic signaling system. *J. Struct. Biol.* 124, 189–200.
- Dong, Y.H., Wang, L.Y., and Zhang, L.H. (2007). Quorum-quenching microbial infections: mechanisms and implications. *Philos. Trans. R. Soc. Lond. B Biol. Sci.* 362, 1201–1211.
- Emsley, P., and Cowtan, K. (2004). Coot: model-building tools for molecular graphics. *Acta Crystallogr. D Biol. Crystallogr.* 60, 2126–2132.
- Engel, C.K., Mathieu, M., Zeelen, J.P., Hiltunen, J.K., and Wierenga, R.K. (1996). Crystal structure of enoyl-coenzyme A (CoA) hydratase at 2.5 angstroms resolution: a spiral fold defines the CoA-binding pocket. *EMBO J.* 15, 5135–5145.
- Engel, C.K., Kiema, T.R., Hiltunen, J.K., and Wierenga, R.K. (1998). The crystal structure of enoyl-CoA hydratase complexed with octanoyl-CoA reveals the structural adaptations required for binding of a long chain fatty acid-CoA molecule. *J. Mol. Biol.* 275, 847–859.
- Feher, V.A., Zapf, J.W., Hoch, J.A., Whiteley, J.M., McIntosh, L.P., Rance, M., Skelton, N.J., Dahlquist, F.W., and Cavanagh, J. (1997). High-resolution NMR structure and backbone dynamics of the Bacillus subtilis response regulator, Spo0F: implications for phosphorylation and molecular recognition. *Biochemistry* 36, 10015–10025.
- Fouhy, Y., Scanlon, K., Schouest, K., Spillane, C., Crossman, L., Avison, M.B., Ryan, R.P., and Dow, J.M. (2007). Diffusible signal factor-dependent cell-cell signaling and virulence in the nosocomial pathogen Stenotrophomonas maltophilia. *J. Bacteriol.* 189, 4964–4968.

- Hamed, R.B., Batchelar, E.T., Clifton, I.J., and Schofield, C.J. (2008). Mechanisms and structures of crotonase superfamily enzymes—how nature controls enolate and oxyanion reactivity. *Cell. Mol. Life Sci.* **65**, 2507–2527.
- He, Y.W., and Zhang, L.H. (2008). Quorum sensing and virulence regulation in *Xanthomonas campestris*. *FEMS Microbiol. Rev.* **32**, 842–857.
- He, Y.W., Wang, C., Zhou, L., Song, H., Dow, J.M., and Zhang, L.H. (2006a). Dual signaling functions of the hybrid sensor kinase RpfC of *Xanthomonas campestris* involve either phosphorelay or receiver domain-protein interaction. *J. Biol. Chem.* **281**, 33414–33421.
- He, Y.W., Xu, M., Lin, K., Ng, Y.J., Wen, C.M., Wang, L.H., Liu, Z.D., Zhang, H.B., Dong, Y.H., Dow, J.M., et al. (2006b). Genome scale analysis of diffusible signal factor regulon in *Xanthomonas campestris* pv. *campestris*: identification of novel cell-cell communication-dependent genes and functions. *Mol. Microbiol.* **59**, 610–622.
- Huang, T.P., and Wong, A.C. (2007). A cyclic AMP receptor protein-regulated cell-cell communication system mediates expression of a FecA homologue in *Stenotrophomonas maltophilia*. *Appl. Environ. Microbiol.* **73**, 5034–5040.
- Hubbard, P.A., Yu, W., Schulz, H., and Kim, J.J. (2005). Domain swapping in the low-similarity isomerase/hydratase superfamily: the crystal structure of rat mitochondrial Delta3, Delta2-enoyl-CoA isomerase. *Protein Sci.* **14**, 1545–1555.
- Kern, D., Volkman, B.F., Luginbuhl, P., Nohaile, M.J., Kustu, S., and Wemmer, D.E. (1999). Structure of a transiently phosphorylated switch in bacterial signal transduction. *Nature* **402**, 894–898.
- Kurimoto, K., Fukai, S., Nureki, O., Muto, Y., and Yokoyama, S. (2001). Crystal structure of human AUH protein, a single-stranded RNA binding homolog of enoyl-CoA hydratase. *Structure* **9**, 1253–1263.
- Leslie, A.G.W. (1992). Joint CCP4 + ESF-EAMCB Newsletter on Protein Crystallography No. 26, 27–33.
- McCoy, A.J., Grosse-Kunstleve, R.W., Adams, P.D., Winn, M.D., Storoni, L.C., and Read, R.J. (2007). Phaser crystallographic software. *J. Appl. Crystallogr.* **40**, 658–674.
- Milton, D.L. (2006). Quorum sensing in vibrios: complexity for diversification. *Int. J. Med. Microbiol.* **296**, 61–71.
- Mingarro, I., Abad, C., and Braco, L. (1995). Interfacial activation-based molecular bioimprinting of lipolytic enzymes. *Proc. Natl. Acad. Sci. USA* **92**, 3308–3312.
- Morris, R.J., Perrakis, A., and Lamzin, V.S. (2002). ARP/wARP's model-building algorithms. I. The main chain. *Acta Crystallogr. D Biol. Crystallogr.* **58**, 968–975.
- Muller-Newen, G., Janssen, U., and Stoffel, W. (1995). Enoyl-CoA hydratase and isomerase form a superfamily with a common active-site glutamate residue. *Eur. J. Biochem.* **228**, 68–73.
- Murshudov, G.N., Vagin, A.A., and Dodson, E.J. (1997). Refinement of macromolecular structures by the maximum-likelihood method. *Acta Crystallogr. D Biol. Crystallogr.* **53**, 240–255.
- Mursula, A.M., van Aalten, D.M., Hiltunen, J.K., and Wierenga, R.K. (2001). The crystal structure of delta(3)-delta(2)-enoyl-CoA isomerase. *J. Mol. Biol.* **309**, 845–853.
- Partanen, S.T., Novikov, D.K., Popov, A.N., Mursula, A.M., Hiltunen, J.K., and Wierenga, R.K. (2004). The 1.3 Å crystal structure of human mitochondrial Delta3-Delta2-enoyl-CoA isomerase shows a novel mode of binding for the fatty acyl group. *J. Mol. Biol.* **342**, 1197–1208.
- Potterton, E., Briggs, P., Turkenburg, M., and Dodson, E. (2003). A graphical user interface to the CCP4 program suite. *Acta Crystallogr. D Biol. Crystallogr.* **59**, 1131–1137.
- Sheldrick, G.M. (2008). A short history of SHELX. *Acta Crystallogr. A* **64**, 112–122.
- Slater, H., Alvarez-Morales, A., Barber, C.E., Daniels, M.J., and Dow, J.M. (2000). A two-component system involving an HD-GYP domain protein links cell-cell signalling to pathogenicity gene expression in *Xanthomonas campestris*. *Mol. Microbiol.* **38**, 986–1003.
- Sola, M., Gomis-Ruth, F.X., Serrano, L., Gonzalez, A., and Coll, M. (1999). Three-dimensional crystal structure of the transcription factor PhoB receiver domain. *J. Mol. Biol.* **285**, 675–687.
- Stock, A.M., Mottonen, J.M., Stock, J.B., and Schutt, C.E. (1989). Three-dimensional structure of CheY, the response regulator of bacterial chemotaxis. *Nature* **337**, 745–749.
- Volkman, B.F., Nohaile, M.J., Amy, N.K., Kustu, S., and Wemmer, D.E. (1995). Three-dimensional solution structure of the N-terminal receiver domain of NTRC. *Biochemistry* **34**, 1413–1424.
- Von Bodman, S.B., Bauer, W.D., and Coplin, D.L. (2003). Quorum sensing in plant-pathogenic bacteria. *Annu. Rev. Phytopathol.* **41**, 455–482.
- Wang, L.H., He, Y., Gao, Y., Wu, J.E., Dong, Y.H., He, C., Wang, S.X., Weng, L.X., Xu, J.L., Tay, L., et al. (2004). A bacterial cell-cell communication signal with cross-kingdom structural analogues. *Mol. Microbiol.* **51**, 903–912.
- Whitehead, N.A., Barnard, A.M., Slater, H., Simpson, N.J., and Salmond, G.P. (2001). Quorum-sensing in Gram-negative bacteria. *FEMS Microbiol. Rev.* **25**, 365–404.
- Zhang, L.H., and Dong, Y.H. (2004). Quorum sensing and signal interference: diverse implications. *Mol. Microbiol.* **53**, 1563–1571.